Available online at www.sciencedirect.com

SciVerse ScienceDirect

Ceramics International 39 (2013) 7557–7561

CERAMICS INTERNATIONAL

www.elsevier.com/locate/ceramint

Effects of Ni doping on structural, optical and dielectric properties of ZnO

Gunjan Srinet, Ravindra Kumar*, Vivek Sajal

Department of Physics & Materials Science & Engineering, Jaypee Institute of Information Technology, Noida 201307, Uttar Pradesh, India

Received 25 January 2013; received in revised form 2 March 2013; accepted 2 March 2013
Available online 14 March 2013

Abstract

Structural, optical and dielectric properties of Ni doped ZnO samples prepared by the solid state route are presented. X-ray diffraction confirmed the substitution of Ni on Zn sites without changing the hexagonal structure of ZnO. NiO phase appeared for 6% Ni doping. Fourier transform infrared measurements were carried out to study phonon modes in Ni doped ZnO. Significant blueshift with Ni doping was observed in UV–visible studies, strongly supported by photoluminescence spectra that show a high intensity UV emission peak followed by the low intensity green emission band corresponding to oxygen vacancies and defects. The photoluminescence analysis suggest that doping of Ni can affect defects and oxygen vacancies in ZnO and give the possibility of band gap tuning for applications in optoelectronic devices. High values of dielectric constant at low frequency and a strong dielectric anomaly around 320 °C were observed.

Keywords: C. Dielectric properties; C. Optical properties; D. ZnO

1. Introduction

ZnO has attracted the scientific community as a multifunctional semiconducting material for optoelectronic devices due to its wide band gap (3.37 eV) and large exciton binding energy (~60 meV) at room temperature [1,2]. Highly crystalline bulk ZnO shows potential applications in short wavelength (blue/UV) light emitting diodes (LEDs) and lasers [3,4]. The interest in studying optical and dielectric properties of Ni doped bulk ZnO is motivated by the need to develop an understanding of the material response to impurities introduced by doping. There are several reports available in the literature on optical and magnetic properties of transition metal doped ZnO [5–7], but still, it is a good candidate for improving the optical and electrical properties, which are crucial for its practical applications. Unique chemical stability of nickel on zinc sites recognizes it as one of the most efficient doping element to improve and tune the optical and electrical properties of ZnO.

On the other hand, dielectric properties of a material are very important which affect many optoelectronic and transport properties. Many applications of ZnO based devices such as LED and UV laser are dependent on the excitonic binding energy which is a function of the dielectric constant. There are few reports in the literature [8,9] on the effect of Co and Ni doping on the static dielectric constant of ZnO at room temperature. Several other groups also studied the effect of transition and non-transition metal doping on dielectric properties of ZnO [10–12]. But results are not conclusive on the dielectric behavior of ZnO. Different values of transition temperatures are reported and the transition is suggested to be either ferroelectric or electrets type [13,14]. Under this scenario, dielectric properties of doped ZnO systems are highly interesting for scientific research.

In the present paper, we study structural, optical and temperature dependent dielectric properties of Ni doped ZnO prepared by the solid state route.

2. Experimental details

Ni doped ZnO samples were prepared by the conventional solid state reaction route. High purity zinc oxide (99.99% purity, Sigma Aldrich) and NiO (99.99% purity, Sigma Aldrich) were used as starting materials. To synthesize $Zn_{1-x}Ni_xO$ (x=0.02, 0.04 and 0.06), appropriate amounts of starting chemicals were ground for 6 h in agate mortar. The

*Corresponding author. Mobile: +91 99 99762428.
E-mail address: ravindrakbhatt@gmail.com (R. Kumar).

0272-8842/$ - see front matter © 2013 Elsevier Ltd and Techna Group S.r.l. All rights reserved.
http://dx.doi.org/10.1016/j.ceramint.2013.03.008

powders were calcined at 600 °C for 12 h in air. Further, samples were ground again and compacted into pellets and sintered at 950 °C for 12 h.

The crystalline structure and the phase purity of samples were confirmed by X-ray diffraction (XRD) measurements (Shimadzu XRD-6000 X-ray diffractometer with CuKα (λ=1.5406 Å) radiation). XRD data was analyzed by the Full Proof Software (Rietveld Methods). Fourier transform infrared spectroscopy (FTIR) was done by using Perkin-Elmer BX-II spectrophotometer through KBr pellet technique in the range 400–4000 cm^{-1}. Absorption spectra were carried out by a Perkin-Elmer Lambda-35 UV–visible spectrometer in the wave-length range 300–800 nm. Photoluminescence (PL) spectra of samples were acquired using xenon flash lamp laser as excitation source by Perkin-Elmer Lambda luminescence spectrophotometer. The dielectric behavior of prepared ceramic samples was studied by impedance analyzer (PSM-1735) using metal–insulator–metal configuration.

3. Results and discussion

3.1. Structural analysis

X-ray diffraction study is performed to investigate the effect of Ni doping on the crystal structure of ZnO. After the final cycle of Rietveld refinement, XRD patterns of $Zn_{1-x}Ni_xO$ (x=0.02, 0.04 and 0.06) samples are shown in Fig. 1. Observed and calculated values were perfectly matching as can be seen from figures. Values of χ^2 were in the range 1.7–2.5, which are good for estimations, as the profile fitting procedure adopted was minimizing χ^2 functions. Rietveld profile refinement of XRD patterns demonstrates that all the Bragg peaks are indexed in the wurtzite type hexagonal structure (space group P63mc) and there is no detectable peak from any other phase upto 4% of Ni but a few traces of NiO (200) phase were detected for x>0.04 which shows that the nickel content

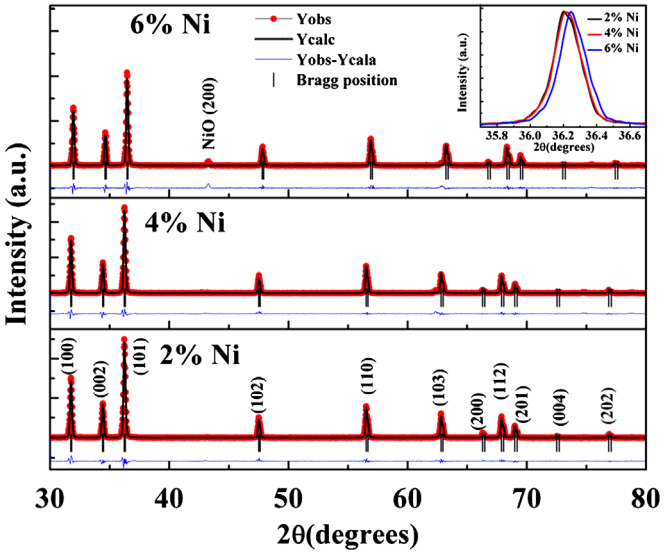

Fig. 1. Reitveld refined XRD patterns of $Zn_{1-x}Ni_xO$ (inset shows the doping-induced peak shift).

x>0.04 is beyond the solid solubility limit of Ni in ZnO, part of Ni ions did not enter the crystalline structure of ZnO and crystallized alone forming NiO grains as indicated in the XRD pattern of 6% doped powder [15]. The refinement of unit cell parameters (Table 1) revealed that cell parameters slightly decreased with increase in Ni concentration, which can be assigned to a smaller ionic radius of Ni^{2+} (0.55 Å) than that of Zn^{2+} (0.60 Å) [16] and to the shifting of peaks to higher angles (shown in the inset of Fig. 1). Bond length shows continuous decrease with doping concentration. Average crystallite sizes vary from 31 to 48 nm which were estimated from the intense ZnO (101) reflection, using Scherrer's relation. All parameters calculated from the Rietveld refinement are concluded in Table 1.

3.2. Optical properties

3.2.1. FTIR studies

Full scan transmittance spectra in the range 400–4000 cm^{-1} are shown in Fig. 2. Low intensity absorption peaks observed around 3400, 2340 and 2925 cm^{-1} are assigned to O–H vibration, CO_2 and C–H mode respectively [17,18]. Absorption peaks at 1580 and 1415 cm^{-1} correspond to asymmetric $\nu_{as}(COO^-)$ and symmetric stretching $\nu_s(COO^-)$ vibrations of acetate species [19]. The water molecule bending vibrational mode (H–O–H) appeared at 1640 cm^{-1} [18]. The IR active characteristic broad band (optical phonon modes) of ZnO is observed in the spectral range 300–600 cm^{-1}. Absorption bands are found to blueshift with Ni doping which shows the substitution of Ni atoms on Zn sites. The observed change in peak positions of ZnO absorption bands reflects that the Zn–O–Zn network is perturbed by the presence of Ni in its environment [17]. For exact positions of Zn–O bands, IR band in the region 400–600 cm^{-1} is shown in the inset (a) of Fig. 2 which is fitted by the Gaussian and shows three bands A_1, A_2 and A_3. The band A_1 at around 443 cm^{-1} corresponds to the E_1 (TO) mode. The bands centered at 485 cm^{-1} (A_2) and 533 cm^{-1} (A_3) are surface phonon modes (SPM) and named as SPM [A_1(TO)] and SPM [E_1(TO)], respectively, which normally appear when prepared particles are smaller than the incident IR wavelength [20]. IR bands corresponding to Zn shows a variation in vibrational frequencies with increase in the doping concentration of Ni, as shown in the inset (b) of Fig. 2. The shift in the band position on doping of Ni may be due to the difference in ionic radii of Zn and Ni as well as

Table 1
Calculated parameter from refinement.

	Lattice parameters			Bond length	R-factors					
	$a=b$ (Å)	c (Å)	V (Å)^3		R_p	R_{wp}	R_{exp}	χ^2	R_b	R_f
2%	3.245	5.196	47.359	1.974	7.9	12.7	9.45	1.7	3.7	2.2
4%	3.244	5.195	47.352	1.974	7.7	13.4	9.26	2.08	3.4	2.12
6%	3.221	5.157	46.353	1.960	13.9	21.2	13.6	2.5	5.15	2.9

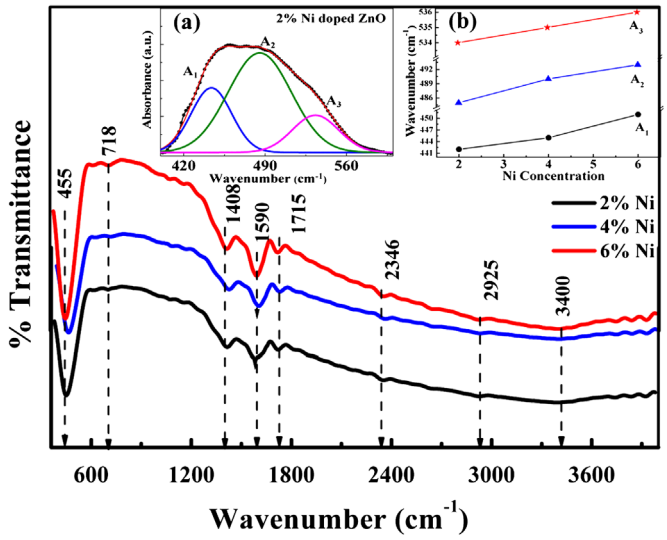

Fig. 2. The full range transmittance spectra of $Zn_{1-x}Ni_xO$. Inset (a) shows zoomed FTIR spectra in the range 400–600 cm^{-1} and (b) shows the variation of IR bands corresponding with Ni content.

Table 2
The IR band and local structure data of Zn Ni–O bonds of $Zn_{1-x}Ni_xO$.

Samples ($Zn_{1-x}Ni_xO$)	Wave number (cm^{-1})	Effective mass (atomic weight)	Force constant (Nm^{-1})	Bond length (Å)
$x=0.02$	443	12.843	148.66	2.52
$x=0.04$	446	12.837	150.62	2.24
$x=0.06$	452	12.832	154.63	2.22

structural changes induced due to the doping [20]. The average bond length of Zn(Ni)–O in $Zn_{1-x}Ni_xO$ system can be determined from the band position of E_1(TO) and by the relation $\nu=(1/2\pi c)(k/\mu)^{1/2}$, where ν is the wave number, c is the velocity of light, k is the average force constant of the Zn (Ni)–O bond and μ is the effective mass of the bond which is given by the relation: $\mu=M_O\times[xM_{Ni}+(1-x)M_{Zn}]/M_O+[xM_{Ni}+(1-x)M_{Zn}]$, where M_O, M_{Zn} and M_{Ni} are atomic weights of O, Zn and Ni, respectively and force constant is related to the average Zn(Ni)–O bond length (Å) by the equation $k=17/r^3$ [21]. Calculated values of effective mass, force constant and bond length are listed in Table 2.

The effective mass of Zn (Ni)–O bond decreased with Ni substitution because of the lower atomic weight of Ni than Zn. Also, a decrease of the average force constant is observed with substitution of Ni which results in an increment in the average Zn (Ni)–O bond length. The variation of the bond length due to Ni substitution is consistent with the trend observed by Rietveld analysis.

3.2.2. UV–visible studies

To study electronic interactions near the band gap region due to doping of Ni, UV–visible absorbance measurements were undertaken. The change in absorption peak due to doping indicates a change in the band structure. It is observed that absorption edges of $Zn_{1-x}Ni_xO$ are at 372, 369 and 367 nm for $x=0.02$, 0.04 and 0.06 respectively. The position of the absorption edge is observed to shift toward lower wavelength side with increase in Ni concentration in ZnO, indicating an increase in the band gap with Ni doping. This blueshift behavior can in principle be explained by the Moss–Burstein band filling effect, which is frequently observed in n-type semiconductors [22,23] (Fig. 3).

3.2.3. Photoluminescence studies

To understand the behavior of surface defects such as oxygen vacancies, room temperature PL emission spectra were recorded at an excitation wavelength of 325 nm which are shown in Fig. 4). A strong emission band appeared in ultraviolet region at around 390 nm (A) due to the

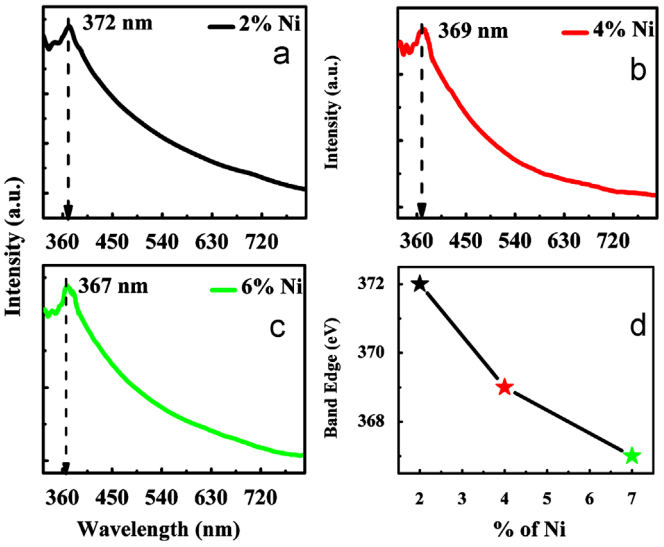

Fig. 3. Absorption spectra of $Zn_{1-x}Ni_xO$ for (a) $x=2\%$, (b) $x=4\%$, (c) $x=6\%$ and (d) shows the variation of band edge with Ni doping.

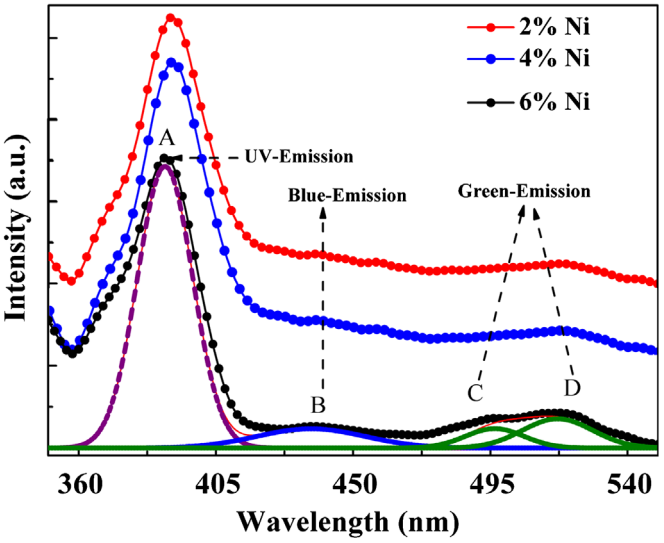

Fig. 4. PL spectra of Ni doped ZnO samples with the Gaussian fit.

recombination of free excitons and is generally assigned as near band edge (NBE) emission band [24].

This NBE peak is found to shift from 392 to 388 nm with increase in doping concentration of Ni. A low intensity broad band with multiple subpeaks (B, C, and D) in the visible emission region spanning the range from green to red is observed (Fig. 4). A variety of deep-level defects have been proposed as possible contributors to the emission in the visible regime. The blue emission peak (B) around 423 nm is probably due to two defect levels, either transition from Zn_i to valence band or transition from the bottom of the conduction band (CB) to interstitial oxygen (O_i) level [18]. The green light (C) emission centered at around 494 nm can be attributed to an oxygen vacancy (V_O) [25] and the emission feature at 520 nm (D) to antisite oxide (O_{Zn}) [26].

3.3. Dielectric properties

Temperature and frequency dependent dielectric constants are shown in Fig. 5 and the inset shows the loss tangent behavior. As shown in the figure, the dielectric constant and loss are strongly temperature and frequency dependent. At room temperature, the value of the dielectric constant is very high and it decreased for high frequencies. The shape of the dielectric curve at the transition temperature is highly asymmetric consisting of a long tail in the lower temperature region and a sharp decrease after transition temperature. The dielectric anomaly around 320 °C was observed to shift toward lower temperature with increasing doping concentration, which is higher than earlier reported values [14] and may be beneficial from the application point of view.

The transition may be ferroelectric phase transition attributed to both order disorder characteristic (whether interaction in direct or phonon mediated between off centered Ni ions) and displacive characteristic (relative translational shift of Zn and O sublattices) [12]. The origin of the possible ferroelectric phase transition could be explained on the basis of the ionic radii difference between the Zn^{2+} and the dopant ions Ni^{2+}. Due to which Ni^{2+} can occupy the off centered position, leading to permanent local electric dipoles and thereby introducing dielectric behavior [13]. Another aspect for the dielectric behavior is the oxygen vacancies. The large value of dielectric constant for all samples at transition point is probably extrinsic due to the space charge formation [27]. The dielectric behavior is still not very clear in this system and further investigations are needed to predict the mechanism behind it.

4. Conclusions

High quality $Zn_{1-x}Ni_xO$ ($x=0.02$, 0.04 and 0.06) samples were synthesized by the solid state route. The phase purity of samples was analyzed by XRD, which shows the phase purity up to 4% of doping concentration, a low intensity peak of NiO is observed for 6% doping concentration. The FTIR spectroscopic measurements show a broad band in the range 600–400 cm^{-1} composed of three distinct peaks assigned to the

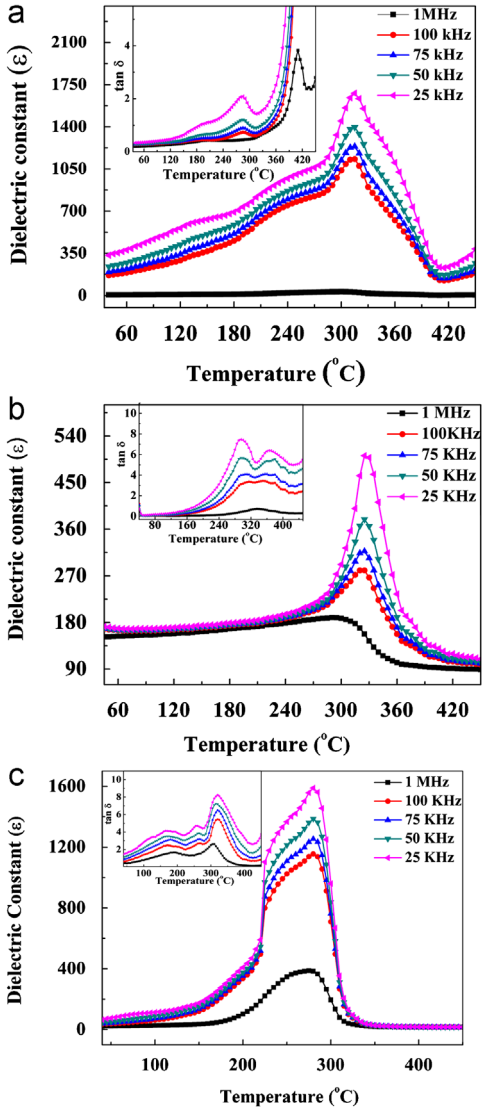

Fig. 5. Dielectric dispersion of $Zn_{1-x}Ni_xO$ ceramics: (a) $x=0.02$, (b) $x=0.04$ and (c) $x=0.06$, as a function of temperature. Inset shows the loss for the corresponding composition.

E_1(TO), SPM A_1(TO) and SPM E_1(TO) modes. A detailed FTIR analysis revealed a decrease in bond length of ZnO with Ni doping which is consistent with XRD results. UV measurement shows the enhancement in the band gap with doping. The blueshift in PL spectra shows strong effect of Ni on ZnO lattice. A transition in the dielectric behavior is observed around 320 °C which is higher than earlier reported values but the transition mechanism is still not clear.

References

[1] U. Ozgur, Ya.I. Alivov, C. Liu, A. Teke, M.A. Reshchikov, S. Dogan, V. Avrutin, S.J. Cho, H. Morkoc, A comprehensive review of ZnO materials and devices, Journal of Applied Physics 98 (2005) 041301.
[2] A.A. Baladin, K.L. Wang, Handbook of Semiconductor Nanostructures and Nanodevices, American scientific publisher, Los Angeles, 2006.
[3] C. Klingshirn, J. Fallert, H. Zhou, J. Sartor, C. Thiele, F. Maier-Flaig, D. Schneider, H. Kalt, 65 years of ZnO research—old and very recent results, Physica Status Solidi B 247 (2010) 1424.

[4] M.D. McCluskey, S.J. Jokela, Defects in ZnO, Journal of Applied Physics 106 (2009) 071101.
[5] Y. Matsumoto, M. Murakami, T. Shono, T. Hasegawa, T. Fukumura, M. Kawasaki, P. Ahmet, T. Chikyow, S. Koshihara, H. Koinuma, Room-temperature ferromagnetism in transparent transition metal-doped titanium dioxide, Science 291 (2001) 854.
[6] H. Yan, J. Johnson, M. Law, R. He, K. Knutsen, J.R. Mckinney, J. Pham, R. Saykally, P. Yang, ZnO nanoribbon microcavity lasers, Advanced Materials 15 (2003) 1907.
[7] S.J. Pearton, D.P. Norton, K. Ip, Y.W. Heo, T. Steiner, Recent progress in processing and properties of ZnO, Progress in Materials Science 50 (2005) 293.
[8] C.K. Ghosh, K.K. Chattopadhyay, M.K. Mitra, Effect of Co doping on the static dielectric constant of ZnO nanoparticles, Journal of Applied Physics 101 (2007) 124911.
[9] C.K. Ghosh, S. Malkhandi, M.K. Mitra, K.K. Chattopadhyay, Effect of Ni doping on the dielectric constant of ZnO and its frequency dependent exchange interaction, Journal of Physics D: Applied Physics 41 (2008) 245113.
[10] H.K. Yadav, K. Sreenivas, V. Gupta, J.F. Scott, R.S. Katiyar, Raman spectroscopy and dielectric studies of multiple phase transitions in ZnO: Ni, Applied Physics Letters 92 (2008) 122908.
[11] Y.C. Yang, C.F. Zhong, X.H. Wang, B. He, S.Q. Wei, F. Zeng, F. Pan, Room temperature multiferroic behavior of Cr-doped ZnO films, Journal of Applied Physics 104 (2008) 064102.
[12] M.K. Gupta, B. Kumar, Enhanced ferroelectric, dielectric and optical behaviour in Li-doped ZnO, Journal of Alloys and Compounds 509 (2011) L-208.
[13] C.W. Zou, L.X. Shao, L.P. Guo, D.J. Fu, T.W. Kang, Ferromagnetism and ferroelectric properties of (Mn, Li) co-doped ZnO nanorods arrays deposited by electrodeposition, Journal of Crystal Growth 331 (2011) 44.
[14] M.K. Gupta, N. Sinha, B. Kumar, Dielectric studies and band gap tuning of ferroelectric Cr-doped ZnO nanorods, Journal of Applied Physics 112 (2012) 014303.
[15] L.N. Tong, X.M. He, H.B. Han, J.L. Hu, A.L. Xia, Y. Tong, Effects of annealing on ferromagnetism of Ni-doped ZnO powders, Solid State Communications 150 (2010) 1112.
[16] X. Huang, G. Li, L. Duan, L. Li, X. Dou, L. Zhang, Formation of ZnO nanosheets with room-temperature ferromagnetism by co-doping with Mn and Ni, Scripta Materialia 60 (2009) 984.
[17] Z. Wei, H. Qiao, H. Yang, C. Zhang, X. Yan, Characterization of NiO nanoparticles by anodic arc plasma method, Journal of Alloys and Compounds 479 (2009) 855.
[18] Y.-M. Hao, S.-Y. lou, S.-M. Zhau, R.-J. Yuan, G.-Y. Zhu, N. Li, Structural, optical, and magnetic studies of manganese-doped zinc oxide hierarchical microspheres by self-assembly of nanoparticles, Nanoscale Research Letters 7 (2012) 100.
[19] B. Dole, V. Mote, V. Huse, Y. Purushotham, M. Lande, K. Jadhav, S. Shah, Structural studies of Mn doped ZnO nanoparticles, Current Applied Physics 11 (2011) 762.
[20] X. Xie, P. Shang, Z. Liu, Y. Lv, Y. Li, W. Shen, Synthesis of nanorod-shaped cobalt hydroxycarbonate and oxide with the mediation of ethylene glycol, Journal of Physical Chemistry C 114 (2010) 2116.
[21] R. El-Mallawany, Theroretical and experimental IR spectra of binary rare earth tellurite glasses, Infrared Physics 29 (1989) 781.
[22] E. Burstein, Anomalous optical absorption limit in InSb, Physical Review 93 (1954) 632.
[23] T.S. Moss, The interpretation of the properties of indium antimonide, Proceedings of the Physical Society London, Section B 67 (1954) 775.
[24] M.H. Huang, Y. Wu, H. Feick, N. Tran, E. Weber, P. Yang, Catalytic growth of zinc oxide nanowires by vapor transport, Advanced Materials 13 (2001) 113.
[25] Z. Yan, Y. Ma, D. Wang, J. Wang, Z. Gao, L. Wang, P. Yu, T. Song, Impact of annealing on morphology and ferromagnetism of ZnO nanorods, Applied Physics Letters 92 (2008) 081911.
[26] B.X. Lin, Z.X. Fu, Y.B. Jia, Green luminescent center in undoped zinc oxide films deposited on silicon substrates, Applied Physics Letters 79 (2001) 943.
[27] D.C. Sinclair, T.B. Adams, F.D. Marrison, A.R. West, $CaCu_3Ti_4O_{12}$: one-step internal barrier layer capacitor, Applied Physics Letters 80 (2002) 2153.